Higher excitation levels of ^{11}B via the ^{10}B$(n,n)^{10}$B and ^{10}B$(n,n')^{10}$B* (0.72, 1.74, 2.15, 3.59, 4.77 MeV) reactions

E. T. Sadowski,* H. D. Knox,† D. A. Resler,‡ and R. O. Lane
Ohio University, Athens, Ohio 45701
(Received 8 January 1990)

Differential cross sections for elastic and inelastic scattering of neutrons from isotopically enriched ^{10}B samples have been measured for incident neutron energies from 3.02 to 6.45 MeV in 250 keV increments and from 7.02 to 12.01 MeV in 500 keV increments. Inelastic angular distributions for scattering to the states in parentheses in ^{10}B have been measured from the indicated energy up to 12.01 MeV: (0.718) from 3.02 MeV; (1.74) from 3.27 MeV; (2.15) from 3.77 MeV; (3.59) from 5.52 MeV; (4.77) from 7.02 MeV. The measurements at 3.02, 3.51, 4.02, and 4.51 MeV were done at nine laboratory angles from 20° to 158° in 17.5° increments with a sample that is isotopically 95.86% ^{10}B. All other distributions measured scattering at 11 laboratory angles from 18° to 158° in 15° increments from a sample that is isotopically 99.49% ^{10}B. A multiple scattering code provided a simulation of the experimental scattering process allowing accurate corrections to the small measured inelastic cross sections. An eight-channel, multilevel R-matrix analysis was performed on the data. Level energies, spins, and parities were deduced for twelve levels above 13 MeV excitation in ^{11}B. Only two definite and three tentative assignments for $T=\frac{1}{2}$ levels had been made previously above 13 MeV. The two definite levels were confirmed. Good agreement between the data and the R-matrix calculation in all analyzed channels was obtained for the proposed structure.

I. INTRODUCTION

Since ^{11}B lies at the center of the $1p$ shell, the prediction of its structure should pose a stringent test for the nuclear shell model, which works best in the neighborhood of closed shells, where only a few valence particles participate in the excitation of the nucleus. ^{11}B, on the other hand, with seven particles above the nearest closed shell and five holes below the next closed shell, has many particles participating in its excitation. It is hoped that results from the measurements reported here will contribute to improvements in our understanding of some of the properties of the shell model as applied to this mass region. Once the structure of ^{11}B at these higher energies is more predictable from the model, then neutron-induced reaction cross sections that are very difficult, if not impossible, to measure experimentally can be calculated more confidently for light nuclei in this region.

Most of the theoretical calculations of the structure of ^{11}B have been performed in the framework of the shell model[1–12] and the rotational model.[13–17] In general, these calculations predict many levels above an excitation energy (E_x) of 14 MeV. The intent of the present work is to study the levels that have the largest spectroscopic amplitudes for the ^{10}B$+n$ and ^{10}B*$+n$ channels, where ^{10}B* refers to excited levels of ^{10}B. This region of excitation is expected to have many broad, overlapping levels because the excitation region of study is very high in ^{11}B and because many particle channels are already open. Therefore, levels in ^{11}B that have small spectroscopic amplitudes for the neutron channels will not be observed in the present neutron cross-section data.

As can be seen in Fig. 1, little spectroscopic information on level properties is definitely known above $E_x=14$ MeV in ^{11}B. In particular, very few spins and parities are known according to the latest compilation,[18] and the situation has not changed appreciably since that time. A previous R-matrix analysis[19] of ^{10}B$(n,n)^{10}$B, ^{10}B$(n,\alpha_0)^7$Li, and ^{10}B$(n,\alpha_1)^7$Li* (0.478 MeV) cross-section data yielded an assignment of $\frac{11}{2}^+$ for the broad level at 14.04 MeV. Zwegliński *et al.*[20] used the direct reactions ^{9}Be$(^3$He$,p)^{11}$B and ^{9}Be$(\alpha,d)^{11}$B to determine an assignment of $\frac{5}{2}^+$ for the $T=\frac{3}{2}$ level at 14.34 MeV. This analysis was only able to determine isospin values, not spins and parities, for remaining levels up to 21.5 MeV excitation. The use of direct reactions to study these high excitation levels in ^{11}B is very difficult since 14 MeV is above the particle separation energies of α (8.665 MeV), t (11.224 MeV), p (11.229 MeV), and n (11.454 MeV). Additional spectroscopic information on levels at E_x greater than 14 MeV has been proposed,[19,21–29] but these analyses have not been confirmed.

The neutron total cross-section measurements of Auchampaugh *et al.*[30] confirmed the existence of several broad resonances above $E_x=14$ MeV or an incident neutron energy (E_n) of 2.8 MeV. Some differential elastic scattering measurements[19,31–36] have been made in the energy range $3<E_n<12$ MeV. For inelastic scattering, data are sparse. Nellis *et al.*[37] measured cross sections for the production of gamma rays from several transitions at 55° for 50 keV$\le E_n \le 5$ MeV and at 14.8 MeV. Day and Walt[38] measured the cross section for the production of the 0.718 MeV gamma ray at 95° from threshold to $E_n=5.2$ MeV. For the other inelastic reactions ($Q=-1.74$, -2.15, -3.59, -4.77 MeV,. . .), even fewer

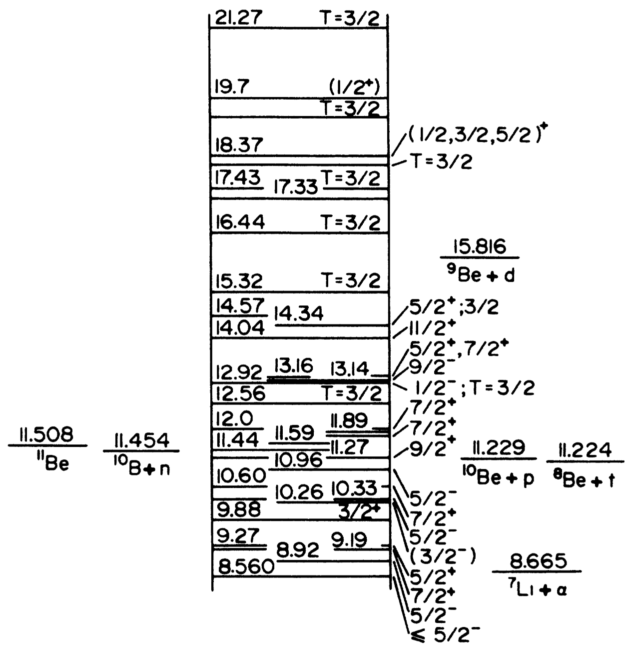

FIG. 1. Previous ^{11}B energy level diagram (Ref. 18) for the region of interest.

data are available. Porter *et al.*[33] measured the differential cross sections for inelastic scattering to the second, third, and fourth excited levels of ^{10}B from threshold to 4.8 MeV. In a recent report by Drosg *et al.*,[36] neutron emission double-differential cross sections were measured for $E_n = 6.0$ and 10.0 MeV. Hopkins and Drake[31] measured differential cross sections for inelastic scattering to the third through seventh excited levels in ^{10}B for $E_n = 7.02$ and 7.55 MeV. The differential cross section for inelastic scattering to the first excited level in ^{10}B was measured only at angles greater than 60° in the center-of-mass frame for 8.0 MeV and at angles greater than 100° for $8.0 < E_n < 14.0$ MeV by Glendinning *et al.*[35] The only other measurement of inelastic differential cross sections published was that by Cookson and Locke[32] at $E_n = 9.72$ MeV; however, only peaks corresponding to scattering to the fourth and 11th excited levels in ^{10}B were resolved. The remaining peaks were analyzed together and the corresponding cross sections were reported as scattering to the second-plus-third levels, fifth-plus-sixth-plus-seventh levels, and eight-plus-ninth-plus-tenth levels. Of all these elastic and inelastic measurements, only Hausladen *et al.*[19] analyzed the measurements in the compound nucleus framework.

The present work studied ^{11}B via neutron elastic and inelastic scattering to the first five excited levels of ^{10}B for $3.0 < E_n < 12.0$ MeV. Angular distributions consisting of 9 or 11 angles were measured. Through the addition of several more channels, i.e., inelastic neutron scattering channels, over a broad energy range, it is hoped that the present work will advance the knowledge of the structure of ^{11}B above $E_x = 14$ MeV by utilizing the R-matrix formalism to extract spectroscopic information (level spins, parities, energies, and widths). The experimental procedure will be discussed in the next section. The following sections will discuss the experimental results, the data analysis and results, comparison to theoretical predictions, and conclusions about the present work.

II. EXPERIMENTAL PROCEDURE

A complete development of the experimental method is given in Ref. 39 and references contained therein. A brief outline of the experimental procedure will be given here.

The Ohio University Tandem Van de Graaff Accelerator produced beams of protons or deuterons of average currents between 2 and 3 μA when the beams were pulsed at a repetition rate of 2.5 MHz and bunched to approximately 1 nsec FWHM. These beams were incident on gas cells 3 cm in length that contained 137 kPa of tritium or deuterium enclosed by windows of 5 μm tungsten foils. The ^{3}H$(p,n)^3$He reaction was used to produce neutrons in the incident neutron energy range $3.0 \le E_n \le 7.5$ MeV. The ^{2}H$(d,n)^3$He reaction produced neutrons in the $7.0 \le E_n \le 12.0$ MeV range. The neutron energy spread for the ^{3}H$(p,n)^3$He reaction was 80–90 keV FWHM. For the ^{2}H$(d,n)^3$He reaction, the neutron energy spread was 100–110 keV.

Two ^{10}B powder scattering samples were employed over the course of this work. The first sample was 67.74 g of 95.86% isotopically pure ^{10}B. Unfortunately, the remaining 4.14% ^{11}B was enough contamination to cause difficulties. The first excited level of ^{11}B is at 2.12 MeV, very close to the energy of the third excited level of ^{10}B, 2.15 MeV. The cross sections for scattering to these two levels were such that the scattering peaks corresponding to these two levels were of the same order of magnitude and experimentally unresolvable. Cross sections for five E_n, 3.0, 3.5, 4.0, 4.5, and 5.0 MeV, were measured using this sample. For the remaining 22 energies, a new sample was prepared. This sample was 64.89 g of 99.49% isotopically pure ^{10}B, so that the scattering peak from the ^{11}B level at 2.12 MeV was no longer a problem. Large samples were required since the inelastic scattering cross sections were expected to be very small. Both samples were contained in thin-walled (0.025 cm thick) cylindrical aluminum cans of radius 2.0 cm and height 4.0 cm. An identical can served for background measurements.

An array of three NE213 liquid scintillator detectors was used. Each scintillator was optically coupled to an RCA 8854 photomultiplier tube. This system provided very effective pulse shape discrimination against gamma rays down to the lowest energies of detectable inelastically scattered neutrons, approximately 800 keV. The distance from the neutron source to the scattering sample was approximately 20 cm, and that from the scattering sample to the detectors was 6 m. The neutron source flux was monitored by a 1-cm-thick×2.5-cm-diam stilbene crystal mounted directly on the face of an RCA 8575 photomultiplier tube at a distance of 88 cm from the gas cell and an angle of 39° relative to the incident charged-particle beam. The remaining details of the experimental procedure such as detector shielding and collimation, cross-section determination, and error calculations are given in Ref. 39.

Due to the large size of the scattering sample, multiple scattering correction factors were quite substantial. The typical multiple scattering correction factor for elastic scattering was 1.20 with an error of 1–1.5 %. The correction factors for the inelastic cross sections varied greatly from angle to angle and energy to energy due mainly to the presence of neutron source contaminants for which correction factors were calculated. A discussion of the many calculations carried out by the multiple scattering correction code MACHO can be found in Refs. 39 and 40. An example of the excellent simulation of the data by the code can be seen in Figs. 2 and 3.

Figure 2 is a probability plot of the energy spectrum of neutrons emanating from a deuterium gas cell at 0° relative to the incident deuteron beam. This spectrum is included in the input to the code MACHO. The small contaminant peaks labeled *a*–*e* were approximately 1% of the main neutron source peak. Since the inelastic scattering cross sections that were measured were approximately 1% of the elastic cross sections, the peaks caused by elastic scattering of these contaminant neutrons were of the same size as the inelastic scattering peaks. Figure 3 displays a typical time-of-flight (TOF) spectrum. The solid line is a plot of the data, and the histograms represent the simulation calculated by the code. The true elastic and inelastic neutron scattering peaks are designated by Q values. Also shown are the contaminant peaks, *a*–*e* from Fig. 2, after having been elastically scattered through 142.5°. The code simulated the experiment very well.

The overall errors in the differential cross sections, including those from the simulation code MACHO, counting statistics, efficiency determinations, etc., were approximately 5% for the elastic cross sections, 10–15 % for all the inelastic cross sections except for the second, and 10–50 % for the second inelastic cross section.

Elastic differential cross-section measurements were performed at 27 incident neutron energies; from 3.02 to 6.46 MeV in 250 keV increments and from 7.00 to 12.00 MeV in 500 keV increments. The Q values of the inelastic scattering and the lowest E_n at which full angular distributions were obtained are -0.72 MeV from 3.02 MeV, -1.74 MeV from 3.51 MeV, -2.15 MeV from 4.02 MeV, -3.59 MeV from 5.52 MeV, and -4.77 MeV from 7.00 MeV. The angular distributions measured using the first ^{10}B sample consisted of nine equally spaced angles (in the laboratory frame) from 20° to 160°. The remaining angular distributions were comprised of 11 angles from 18° to 158°. Along with comparing elastic cross-section values from the present work and previous measurements, ^{12}C elastic cross sections were also measured and compared to previous measurements to ensure the accuracy of the experimental apparatus.

III. EXPERIMENTAL RESULTS

Figures 4–6 show representative angular distributions from the present work for elastic and inelastic neutron scattering from ^{10}B. Cross sections and angles are given in the center-of-mass frame, while the indicated energies are incident neutron energies in the laboratory frame. The lines through the data are five-polynomial Legendre

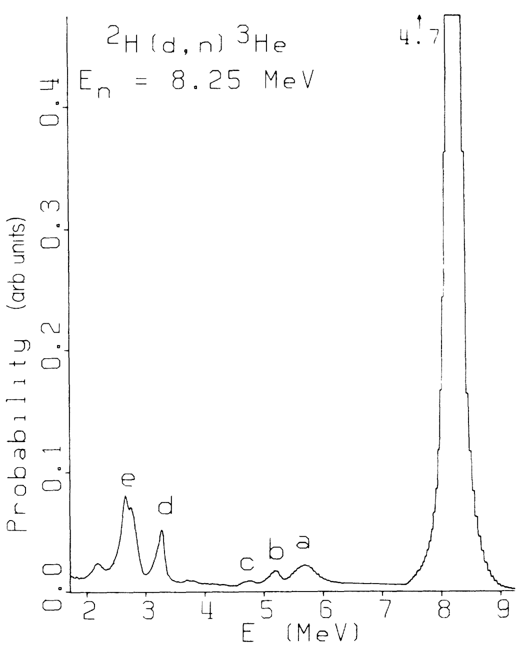

FIG. 2. Energy probability spectrum at 0° for the ^{2}H$(d,n)^{3}$He reaction. The peaks labeled *a*–*e* are source contaminants and are of the order of 1% of the main peak.

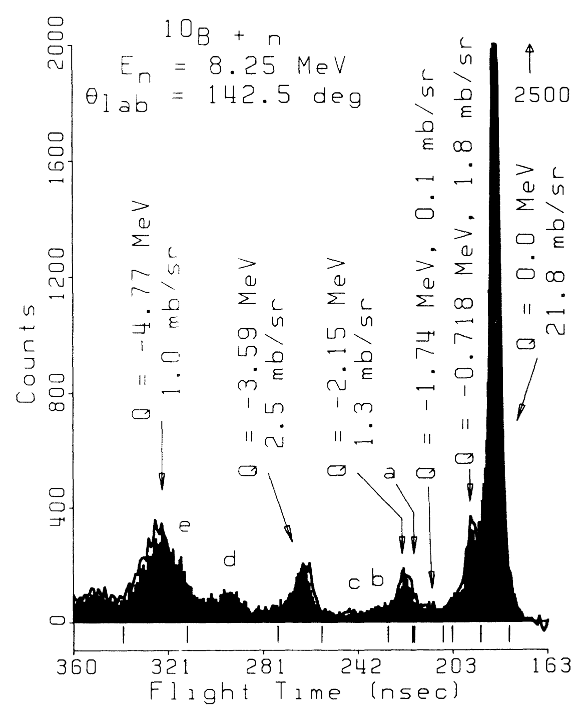

FIG. 3. The MACHO time-of-flight simulation from using Fig. 2 as the energy input. The peaks labeled *a*–*e* correspond to the peaks from Fig. 2 after being scattered elastically through 142.5°.

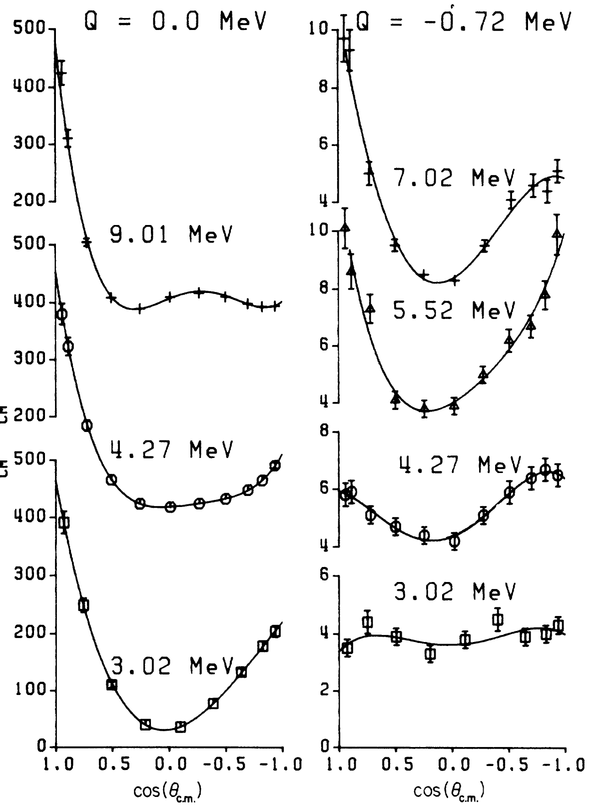

FIG. 4. Representative elastic and first inelastic angular distributions. The lines through the data are five-polynomial Legendre fits.

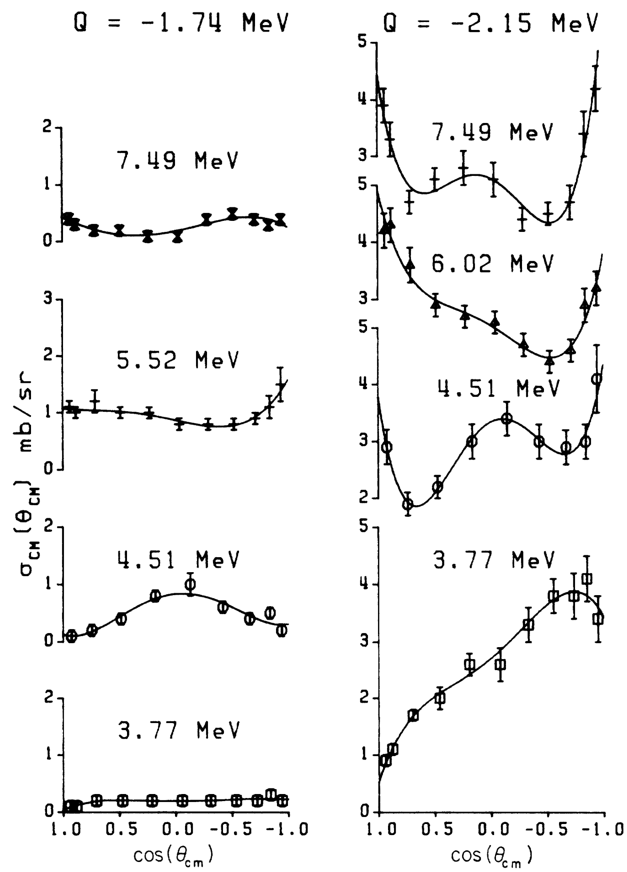

FIG. 5. Representative second and third inelastic angular distributions. The lines through the data are five-polynomial Lengendre fits.

fits. For energies shown here, higher-order Legendre polynomial coefficients were statistically zero and their omission did not affect either the quality of the fit or the values of the lower-order coefficients. The variation of the Legendre polynomial coefficients B_L with E_n in the laboratory frame can be seen in Figs. 7–12. From these plots, it can be seen that the present data agree well with most all of the previous measurements. The solid line is the R-matrix fit to the data and will be discussed in the next section.

As can be seen in Fig. 7, the structure of the elastic cross section changes from broad resonances for $E_n < 6$ MeV to very broad resonances between 6 and 8 MeV and finally to very little, if any, variation with energy for $E_n > 8$ MeV. The inelastic cross sections show a similar behavior, except that the magnitude is very, very small for $E_n > 8$ MeV. The broad nature of the resonances is a manifestation of the particular structure of ^{11}B, in contrast to its $1p$ shell neighbors, ^{8}Li and ^{10}Be on one side and ^{12}B, ^{13}C, and ^{14}C on the other, whose formations via the neutron channel show rather narrower resonances at modest energies above their neutron separation energies. In these nuclei the neutron channel usually opens at considerably lower excitation energies than the other particle channels. This makes the neutron interaction a single-channel process with narrow level widths for a substantial interval of energy before other reactions open up at higher energies causing the total widths, i.e., the measured widths of the resonances, to increase. In ^{11}B, on the other hand, the neutron separation energy, 11.454 MeV, is much higher than the separation energy for the alpha particle (8.665 MeV), as well as being higher than the separation energies for the triton (11.224 MeV) and the proton (11.229 MeV). With all these charged-particle channels already open and contributing their own partial widths to the total width of the resonance, broad neutron resonances are expected to result. For $E_n \approx 5$ MeV, the deuteron channel also becomes available as another mode of decay resulting in yet another partial width being added to the total width of the resonances. Also, as the excitation energy increases, the higher penetrabilities of the emitted particles result in further broadening. After a certain point, say $E_n \approx 9$ MeV or so, these very broad levels overlap to such an extent that their individuality is lost, and the cross section appears to have no variation with energy. The region $E_n \geq 10$ MeV may well be characterized as the beginning of applicability of the optical model in which such overlap is a basic premise. The present R-matrix analysis concentrated on the region below $E_n = 9$–10 MeV. Broad levels that were assumed in the R-matrix analysis at higher energies in order to give proper background effects in fitting the data below this

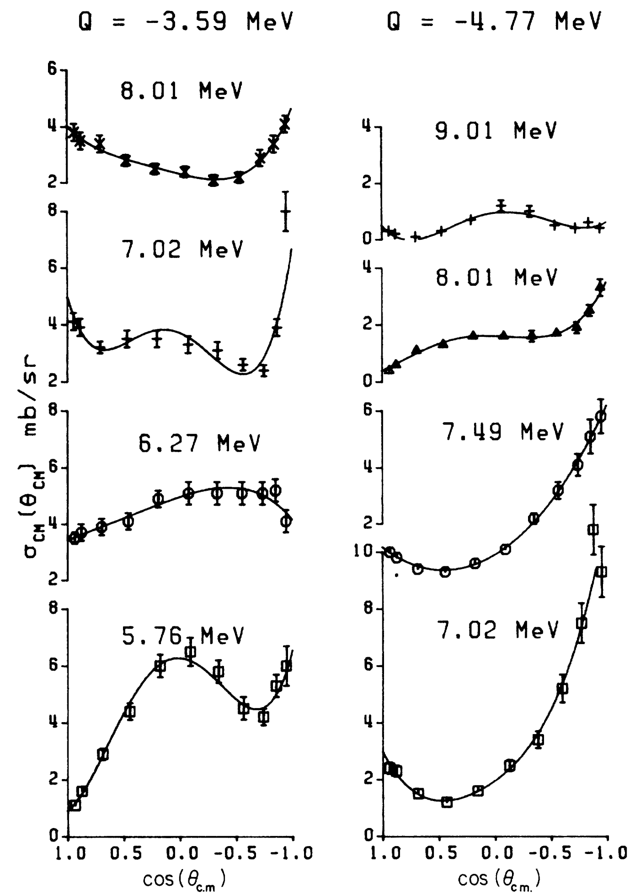

FIG. 6. Representative fourth and fifth inelastic angular distributions. The lines through the data are five-polynomial Legendre fits.

energy should be interpreted only as indications of the nature of scattering amplitudes present at higher energies rather than claims to definite assignments of levels at those energies.

IV. *R*-MATRIX ANALYSIS OF THE DATA

Along with elastic and inelastic scattering to the first five excited levels of ^{10}B, ^{10}B$(n,\alpha_0)^7$Li, and ^{10}B$(n,\alpha_1)^7$Li* (0.478 MeV) data for 0.2 MeV $\leq E_n \leq 7.58$ MeV were analyzed. The only other neutron-induced reaction for which data were available was the ^{10}B$(n,t)2\alpha$ reaction. While tritium production has been measured from thermal neutron energies to 14 MeV, the relative importance of the immediate three-particle breakup and the sequential breakup processes through ^{7}Li and ^{8}Be intermediate states are unclear. Antolkovic *et al.*[41] have placed an upper limit of 10 mb on the immediate breakup reaction for $E_n = 14.4$ MeV. This value is 10% of the cross section for the sequential processes. Over the energy range of the present work the elastic cross section is more than an order of magnitude greater than the tritium production cross section, and further, the inelastic cross sections (except for scattering to the second excited level of ^{10}B) are several times the tritium production cross section. Therefore, the ^{10}B$(n,t)2\alpha$ reaction channel was not included in the present analysis.

The channel radii a_c were chosen according to the relation $a_c = a_0(A_1^{1/3} + A_2^{1/3})$, where A_1 and A_2 are the mass numbers of the two particles in reaction channel c. The choice of $a_0 = 1.20$ fm resulted from examining the R-matrix prediction of hard-sphere scattering and the available optical model parameters for the real potential well depth, the radius, and the diffuseness parameter. A Woods-Saxon form was used for the shape of the potential. The potential was plotted as a function of radius using parameters from various optical model analyses[32,33,35,42,43] for E_n within the range of the present study. For each choice of a_0, 1.20, 1.30, 1.40, and 1.50 fm, the amount of the potential well that was outside the corresponding value for a_c, i.e., beyond the region of interaction for this channel, was noted. Also noted was the degree of departure from the data for high-order B_L for the R-matrix calculation for hard-sphere scattering. The choice of $a_0 = 1.20$ fm put only a very small amount of the nuclear interaction outside the channel boundary, while maintaining values of B_6 ($l=3$) in close agreement with the data. If a larger a_0 was used, the B_6 coefficient for hard-sphere scattering was much larger than the data warranted. The channel radius chosen in this manner for ^{10}B$+n$ was 3.78 fm, and for ^{7}Li$+\alpha$, it was 4.20 fm.

Since the region of study of the present work spans 9 MeV, it is not surprising that early in the fitting process constant R-matrix terms for backgrounds were found to be inadequate. Following the method of Koehler[44] and Resler,[45] no constant background was used. Instead, very broad background levels were placed into the R-matrix calculation above $E_x = 25$ MeV ($E_n = 15$ MeV). It is not claimed that these broad levels actually exist at these particular energies; the only claim is that these particular types of J^π strengths exist somewhere near this energy region, and these levels give convenient energy-dependent backgrounds close to that exhibited by the data. No background was needed for the (n,α_1) channels, while a single $\frac{5}{2}^+$ level supplied all the necessary (n,α_0) background. The background level parameters are shown in Table I.

Most of the values of the $\gamma_{\lambda c}$ in Table I are reasonable in comparison to the Wigner limit,[46] $\gamma_{\lambda c}^2 = 3\hbar^2/2\mu a_c^2$. In the present case, this limit is approximately 5 MeV for the ^{10}B$+n$ channel and 1.4 MeV for the ^{7}Li$+\alpha$ channel. The limit applies to the available strength for a particular J^π in a single shell.[47] The predicted value should be accurate to within a factor of 2 or so.[48] For $J^\pi = \frac{5}{2}^+$, resonances were added such that the sum of the $\gamma_{\lambda c}^2$ was approximately four times the Wigner limit. Allowing for the factor of 2 uncertainty, this may mean that configurations involving two shells that are $2\hbar\omega$ apart in energy (for the correct parity) would be needed. Therefore, to describe accurately this region of ^{11}B with the shell model, $1\hbar\omega$ and $3\hbar\omega$ excitations to the $2s$-$1d$ and $3s$-$2d$-$1g$ shells may be important.

The single level approximation[49] gives

$$\Gamma_{\lambda c} = 2P_c\gamma_{\lambda c}^2$$

TABLE I. Background R-matrix parameters.

J^π	E_x (MeV)	E_λ (MeV)	$\gamma_{\lambda c}$ (MeV$^{1/2}$) $s_{1/2}$	$p_{1/2}$	$p_{3/2}$	$d_{3/2}$	$d_{5/2}$	$p_1(n,\alpha_0)$
$\frac{3}{2}^-$	25.1	13.9			1.5			
$\frac{5}{2}^+$	26.2	14.8	2.0					1.5
$\frac{5}{2}^-$	26.3	14.9			1.0			
$\frac{7}{2}^+$	26.3	14.7	1.0					
$\frac{7}{2}^-$	26.3	14.9		1.0				
$\frac{9}{2}^+$	25.2	14.1				1.0		
$\frac{9}{2}^+$	26.7	15.5					1.0	
$\frac{9}{2}^-$	25.4	14.3			1.0			

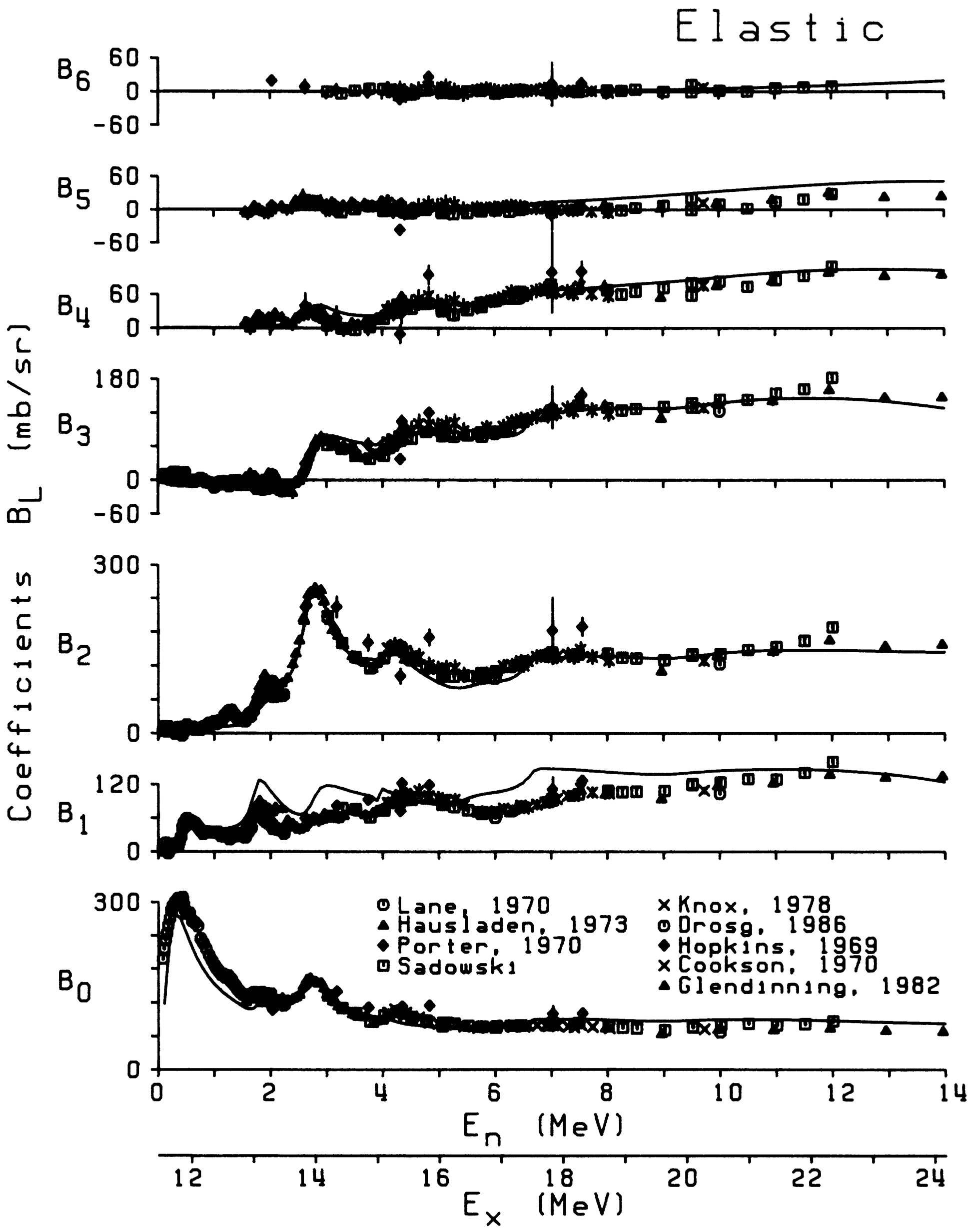

FIG. 7. Legendre polynomial coefficients for the expansion $\sigma_{\mathrm{c.m}}(\theta_{\mathrm{c.m}}) = \sum_L B_L P_L(\cos\theta_{\mathrm{c.m}})$ for the differential elastic scattering cross section plotted as a function of incident laboratory energy E_n. The solid curve is the final R-matrix fit to the data. The parameters are listed in Tables I–V. The errors for the present data are less than the size of the symbol unless otherwise shown.

and

$$E_\lambda = (E_x - E_{sep}) + \sum_c (S_c - B_c)\gamma^2_{\lambda c} ,$$

where $\Gamma_{\lambda c}$ is the observed width in MeV of level λ in reaction channel c, P_c is the penetrability of the light particle in channel c, $\gamma^2_{\lambda c}$ is the reduced width, E_λ is the level energy, E_{sep} is the particle separation energy in the ^{11}B compound nucleus, and S_c and B_c are the shift factor and boundary condition for channel c. The B_c were set equal to their respective S_c at $E_n = 7.5$ MeV, the midpoint of the present range of study. These equations were used to relate E_x and $\Gamma_{\lambda c}$ to the E_λ and $\gamma_{\lambda c}$ of the R-matrix calculations. The results of this analysis are summarized in Tables 2–5 and Figs. 7–14 and will be discussed in the following sections.

A. $E_x < 13$ MeV ($E_n < 1.7$ MeV)

Since the present study concentrated primarily on the levels at much higher energies, and further since the region of low neutron energies was investigated extensively earlier,[19] only the dominant effects by some levels in this region on the fitting at much higher energies was considered.

This region does not involve any appreciable amount of the inelastic channels, even though the first inelastic group is energetically allowed. The cross section for scattering to the first excited state in ^{10}B, as measured by the $(n,n'\gamma)$ work of Nellis *et al.*[37] is very, very small. Therefore, only the elastic, (n,α_0) and (n,α_1) channels were analyzed, and no new information was learned in this region. Some reduced widths and level energies were

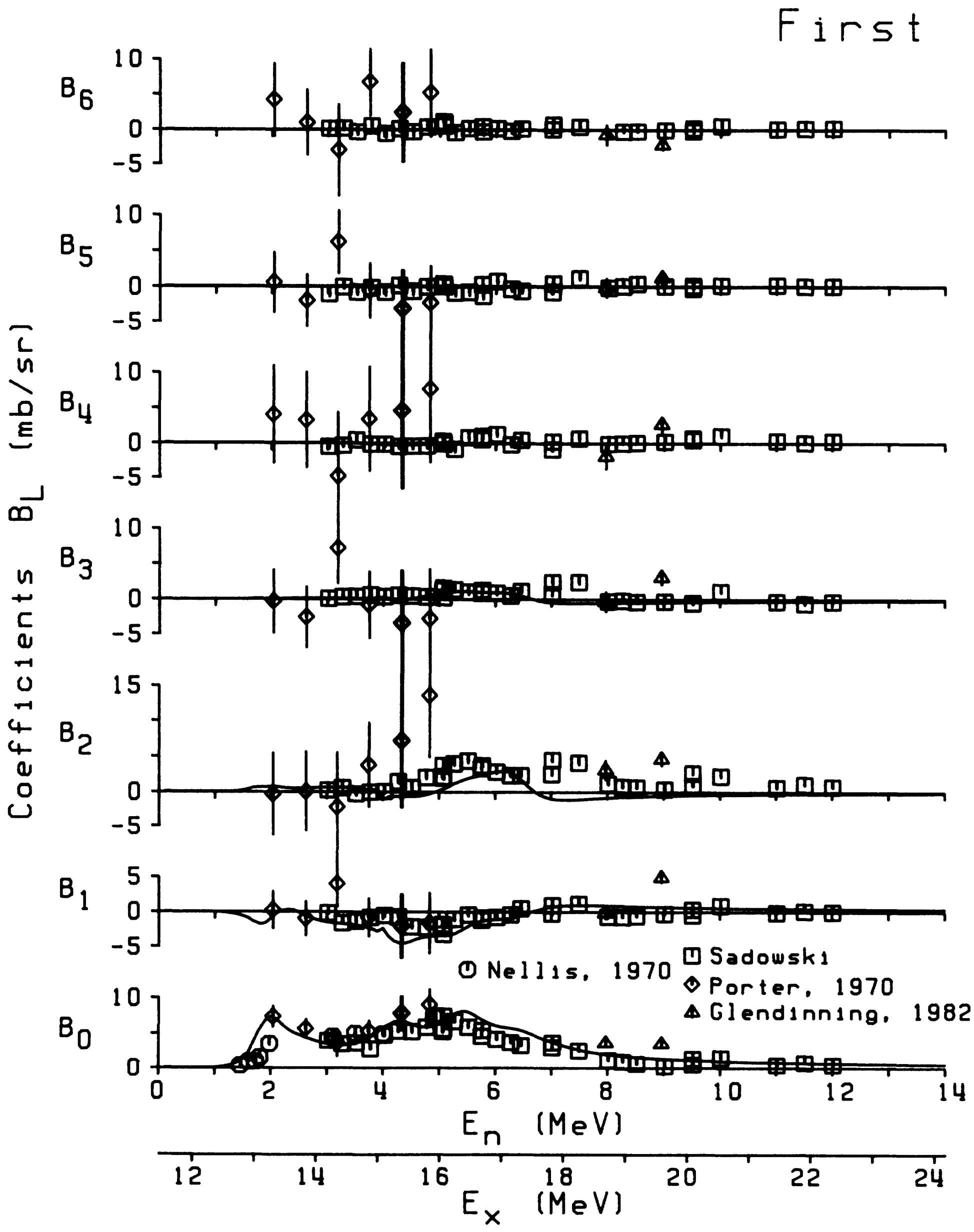

FIG. 8. Legendre polynomial coefficients for inelastic scattering to the first excited state of ^{10}B. See caption for Fig. 7.

adjusted from the previous analyses[19,50] to account for the interference between these levels and newly assigned levels above $E_x = 13$ MeV. The dominant structures at this low E_n are the large B_0 peak in the elastic channel resulting from the $\frac{7}{2}^+$ level at 11.79 MeV, and the end of the $1/v$ cross section in the α_1 channel caused[50] by the interference between the bound $\frac{7}{2}^+$ at 10.60 MeV and the unbound $\frac{7}{2}^+$ at 11.79 MeV. The major shortcoming of the fit in this region is the inversion of the fit relative to the data in B_2 in the α channels at $E_x = 11.94$ MeV. The previous analysis[19] did not have the differential data available to it. While the B_1 coefficient, produced by interference between the $\frac{5}{2}^-$ level at 11.94 MeV and the $\frac{7}{2}^+$ level at 11.79 MeV, was fitted well by making the $\frac{5}{2}^-$ reduced width amplitude in the α_1 channel negative, nothing that was attempted correctly calculated the polarity of the B_2 data, although many combinations of negative $\gamma_{\lambda c}$ of all the levels including background levels were attempted. The other level included in the fit in this region was a $\frac{5}{2}^+$ at 11.60 MeV. See Refs. 19 and 50 for more discussion on these levels.

B. $13 < E_x < 14.5$ MeV ($1.7 < E_n < 3.4$ MeV)

The $\frac{9}{2}^-$ level at 13.12 MeV and the $\frac{11}{2}^+$ level at 14.0 MeV were both thoroughly discussed by Hausladen *et al.*[19] The present work confirmed these assignments. The newly measured inelastic channels were of no help in the further study of these two levels due their high spins. In this region, only the cross section for scattering to the first excited level in ^{10}B was appreciable, but the penetra-

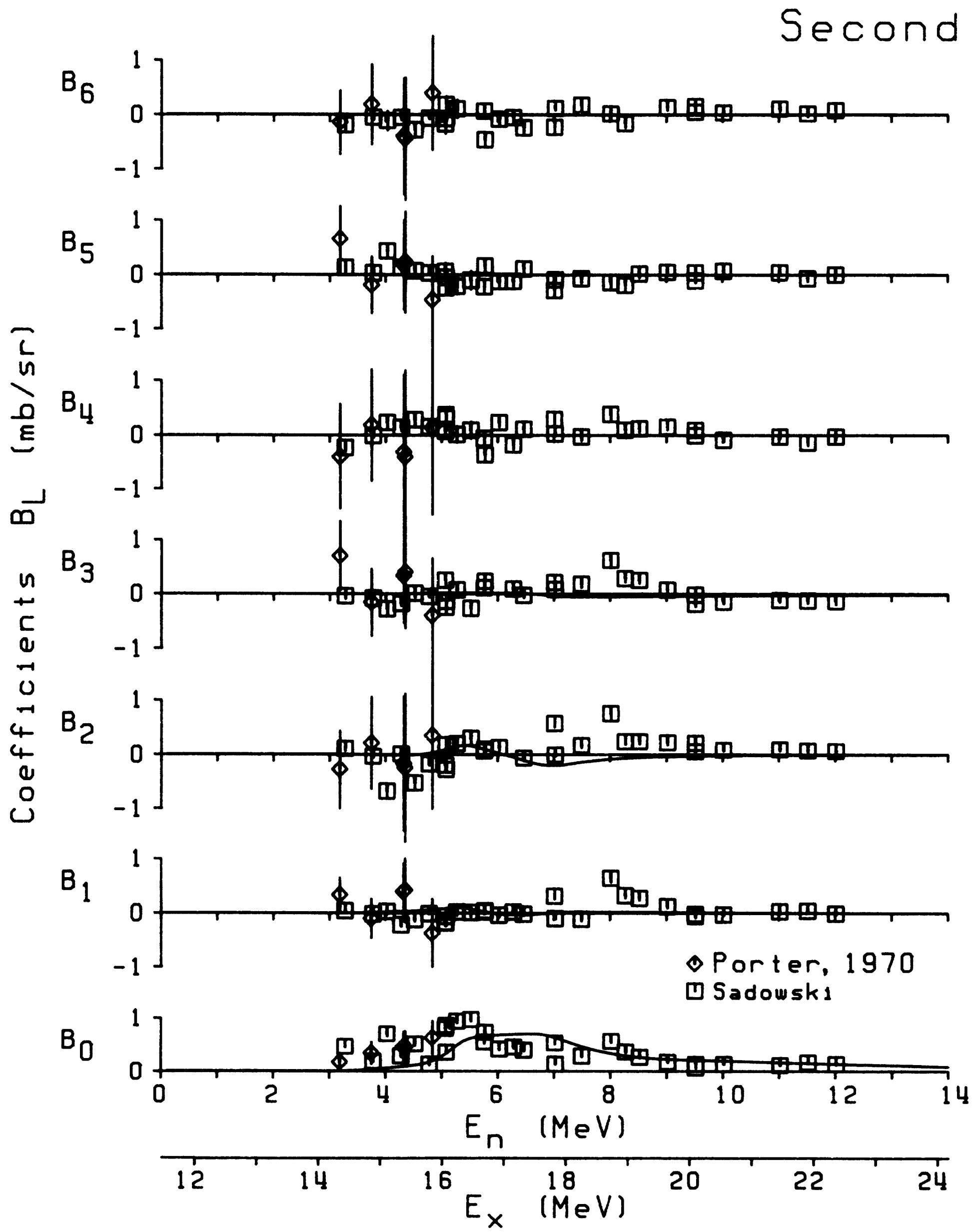

FIG. 9. Legendre polynomial coefficients for inelastic scattering to the second excited state of ^{10}B. See caption for Fig. 7.

TABLE II. Elastic neutron R-matrix parameters.

			$\gamma_{\lambda c}$ (MeV$^{1/2}$)				
E_x (MeV)	J^π	E_λ (MeV)	$s_{1/2}$	$p_{1/2}$	$p_{3/2}$	$d_{3/2}$	$d_{5/2}$
10.6	$\frac{7}{2}^+$	−2.07	−0.346				
11.6	$\frac{5}{2}^+$	−1.06	0.081				
11.8	$\frac{7}{2}^+$	−1.15	1.205				
11.9	$\frac{5}{2}^-$	0.30		0.062	0.340		
13.1	$\frac{9}{2}^-$	−0.30			0.436		
13.2	$\frac{5}{2}^+$	0.44				0.331	0.331
13.7	$\frac{3}{2}^+$	1.31				0.892	0.892
13.9	$\frac{5}{2}^-$	1.54		0.288	0.288		
14.0	$\frac{11}{2}^+$	0.52					1.413
15.2	$\frac{7}{2}^+$	3.28	0.285			0.400	0.400
15.6	$\frac{5}{2}^+$	1.02	0.570			0.793	0.793
15.8	$\frac{9}{2}^-$	3.41			0.114		
16.5	$\frac{7}{2}^-$	2.39		−0.429	0.429		
16.9	$\frac{5}{2}^-$	5.20		−0.417	−0.417		
17.8	$\frac{7}{2}^-$	5.16			−0.395		
17.9	$\frac{7}{2}$	5.79		−0.395	−0.395		
18.1	$\frac{9}{2}^+$	5.71				0.269	0.269
19.5	$\frac{5}{2}^-$	8.35		0.364	0.364		

TABLE III. Inelastic neutron R-matrix parameters.

					$\gamma_{\lambda c}$ (MeV$^{1/2}$)			
E_x (MeV)	J^π	$s_{1/2}$	$p_{1/2}$	$p_{3/2}$	$d_{3/2}$	$d_{5/2}$	$f_{5/2}$	$f_{7/2}$
13.2	$\frac{5}{2}^+$				0.771(n_1)	0.771(n_1)		
13.7	$\frac{3}{2}^+$	0.357(n_1)						
13.9	$\frac{5}{2}^-$			0.677(n_1)				
15.2	$\frac{7}{2}^+$					−0.477(n_1)		
						0.897(n_3)		
15.6	$\frac{5}{2}^+$				0.675(n_1)	0.675(n_1)		
						0.250(n_2)		
					1.267(n_3)	1.267(n_3)		
15.8	$\frac{9}{2}^-$							0.379(n_1)
								0.549(n_3)
16.5	$\frac{7}{2}^-$			0.738(n_4)			−1.235(n_1)	−1.235(n_1)
								1.158(n_2)
							0.421(n_3)	0.421(n_3)
16.9	$\frac{5}{2}^-$			0.437(n_1)			0.979(n_2)	
				−0.180(n_3)				
			−0.462(n_4)	−0.462(n_4)				
17.8	$\frac{9}{2}^-$				1.006(n_5)		−1.224(n_1)	
							−1.297(n_3)	
							0.522(n_4)	0.522(n_4)
17.9	$\frac{7}{2}^-$			0.547(n_4)			0.866(n_1)	0.866(n_1)
			0.503(n_5)	0.503(n_5)				0.803(n_2)
							1.297(n_3)	1.297(n_3)
18.1	$\frac{9}{2}^+$					0.369(n_4)		
					0.914(n_5)	0.914(n_5)		
19.5	$\frac{5}{2}^-$		−0.449(n_4)	−0.449(n_4)				

TABLE IV. Alpha R-matrix parameters.

E_x (MeV)	J^π	p_1	d_2	$\gamma_{\lambda c}$ (MeV$^{1/2}$) f_3	g_4	h_5
10.6	$\frac{7}{2}^+$			$0.232(\alpha_0)$		
				$0.642(\alpha_1)$		
11.6	$\frac{5}{2}^+$	$0.348(\alpha_0)$		$0.767(\alpha_1)$		
11.8	$\frac{7}{2}^+$			$0.048(\alpha_1)$		
				$0.701(\alpha_1)$		
11.9	$\frac{5}{2}^-$		$0.224(\alpha_0)$			
			$-0.284(\alpha_1)$			
13.1	$\frac{9}{2}^-$				$0.920(\alpha_0)$	
					$0.499(\alpha_1)$	
13.2	$\frac{5}{2}^+$			$0.390(\alpha_0)$		
				$0.321(\alpha_1)$		
13.7	$\frac{3}{2}^+$	$0.234(\alpha_0)$				
		$0.347(\alpha_1)$				
13.9	$\frac{5}{2}^-$		$0.188(\alpha_0)$			
			$0.202(\alpha_1)$			
14.0	$\frac{11}{2}^+$					$0.618(\alpha_0)$
						$0.373(\alpha_1)$
15.2	$\frac{7}{2}^+$			$0.146(\alpha_0)$		
				$0.221(\alpha_1)$		
15.6	$\frac{5}{2}^+$			$0.146(\alpha_0)$		
				$0.313(\alpha_1)$		
15.8	$\frac{9}{2}^-$				$0.098(\alpha_0)$	
					$0.153(\alpha_1)$	

bility for neutrons with $l_n=3$ required for the decay was only 0.000 78, so the cross section is considered to come from nearby lower spin levels in ^{11}B. The E_n was barely above threshold for scattering to the second and third excited levels of ^{10}B, so the penetrabilities were essentially negligible for decay of the $\frac{11}{2}^+$ level via $l_n=6$ and $l_n=4$. Therefore, the three new assignments made for this region relied primarily on the fitting of the cross-section data for scattering to the first excited level in ^{10}B.

Hausladen *et al.*[19] made an assignment of $\frac{5}{2}^+$ or $\frac{7}{2}^+$ for the level at 13.17 MeV. In the present work, the large rise in the first inelastic B_0 could only be fitted by a $\frac{5}{2}^+$ level. All spins and parities for $l_n \le 3$ were attempted, not only $\frac{5}{2}^+$ or $\frac{7}{2}^+$. A level near $E_x=12.71$ MeV in the mirror nucleus ^{11}C has been identified by Rihet[28] as a $\frac{5}{2}^+$ through an R-matrix analysis of ^{10}B$+p$. Many theoretical calculations[3,8,10–12,24,51] indicate a $\frac{5}{2}^+$ level in this vicinity. The present value of the dimensionless reduced width amplitude $\theta_{\lambda c}$ for the neutron elastic channel is 0.213, much larger than the theoretical prediction from the shell model calculation of Teeters and Kurath[8] 0.031. Those authors also calculated a $\theta_{\lambda c}$ for the first inelastic reaction to be 0.093, again much lower than the present value of 0.496. A possible explanation for this would be that the theoretical calculation predicts other levels in the area in addition to this level sharing the total strength, while the present work puts all the strength into one level.

In the region $2.5<E_n<3.5$ MeV, the B_0 for scattering to the first excited level in ^{10}B and that for the (n,α_1) channel can be fitted by two levels, one positive parity and one negative parity. Again, all possible J^π for $l_n \le 3$ were attempted, and only a $\frac{3}{2}^+$ at 13.7 MeV and a $\frac{5}{2}^-$ at 13.9 MeV, provided enough cross section for the B_0 as well as reasonable fits to all the elastic coefficients as well as to the B_0 for (n,α_0). Teeters and Kurath have predicted a $\frac{3}{2}^+$ at 12.8 MeV. Brown[12] has predicted a $\frac{3}{2}^+$ at 13.68 MeV and a $\frac{5}{2}^-$ at 13.99 MeV. A $\frac{5}{2}^-$ in the area of 13.9 MeV has been predicted by several calculations.[2,13,15,24,52] Cohen and Kurath[2] have calculated spectroscopic factors for negative parity levels up to 19.7 MeV. Their $\theta_{\lambda\,\mathrm{elas}}$ for a $\frac{5}{2}^-$ at 14.40 MeV of 0.153 agrees well with 0.185 from the present work.

C. $14.5<E_x<17.0$ MeV ($3.4<E_n<6.1$ MeV)

In this energy region, the cross sections for scattering to the second, third, and fourth excited levels of ^{10}B also become sizable. The Legendre coefficients for all of the first four inelastic scattering cross sections show a similar behavior. B_0 rises for energies just above threshold, forms a wide peak, then decreases slowly. The higher-order coefficients for all the reactions also show broad structure, though not as broad as the B_0 coefficients. Each elastic coefficient from B_0 to B_4 shows a single, broad resonance followed by a broad dip. Combined with the fact that the resonances are seen in the odd as well as the even coefficients and that no single level was able to fit the amplitude of any of the coefficients, all this broad structure is indicative of several broad levels interfering to cause the peaks as well as the dips. Since the levels are so broad and interfere with each other so much, changing the E_λ of the levels by 200 keV does not alter very much the agreement between the R-matrix fit and the data. For this reason, the energies quoted can be taken to have errors of plus or minus 0.2 MeV. The α channels yield little information in this energy region and above. The only discernible structure in this region of the (n,α) cross section is a broad resonance much like the B_0 of the inelastic cross sections. Since no (n,α) angular distributions exist above $E_n = 1.2$ MeV and the alpha particle energy is so high that the penetrabilities for alphas with all angular momenta are reasonably high, the α channels will not discriminate very well between various J^π possibilities for a particular level.

Five levels were identified in this region, $\frac{7}{2}^+$ at 15.2 MeV, $\frac{5}{2}^+$ at 15.6 MeV, $\frac{9}{2}^-$ at 15.8 MeV, $\frac{7}{2}^-$ at 16.5 MeV, and $\frac{5}{2}^-$ at 16.9 MeV. All of these levels had unique effects on the R-matrix fit. In all cases, all possible J^π values for $l_n \le 3$ were attempted at each energy. The final

TABLE V. Partial widths of R-matrix levels.

		$\Gamma_{\lambda c} = 2P_c\gamma_{\lambda c}^2$ (MeV)							
E_x (MeV)	J^π	Γ_{n_0}	Γ_{n_1}	Γ_{n_2}	Γ_{n_3}	Γ_{n_4}	Γ_{n_5}	Γ_{α_0}	Γ_{α_1}
10.6	$\frac{7}{2}^+$							0.003	0.006
11.6	$\frac{5}{2}^+$	0.004						0.296	0.100
11.8	$\frac{7}{2}^+$	1.339						0.002	0.113
11.9	$\frac{5}{2}^-$	0.001						0.080	0.090
		0.030							
13.1	$\frac{9}{2}^-$	0.200						0.275	0.050
13.2	$\frac{5}{2}^+$	0.020	0.033					0.194	0.116
		0.020	0.033						
13.7	$\frac{3}{2}^+$	0.250	0.250					0.125	0.125
		0.250							
13.9	$\frac{5}{2}^-$	0.125	0.500						
		0.125							
14.0	$\frac{11}{2}^+$	0.800						0.045	0.010
15.2	$\frac{7}{2}^+$	0.250	0.125		0.125			0.062	0.125
		0.125							
		0.125							
15.6	$\frac{5}{2}^+$	1.000	0.300	0.025	0.380			0.068	0.278
		0.500	0.300		0.380				
		0.500							
15.8	$\frac{9}{2}^-$	0.031	0.015		0.006			0.015	0.031
16.5	$\frac{7}{2}^-$	0.500	0.250	0.100	0.010	0.500			
		0.500	0.250		0.010				
16.9	$\frac{5}{2}^-$	0.500	0.500	0.100	0.063	0.250			
		0.500				0.250			
17.8	$\frac{9}{2}^-$	0.500	0.500		0.250	0.012	1.000		
						0.012			
17.9	$\frac{7}{2}^-$	0.500	0.250	0.125	0.250	0.500	0.250		
		0.500	0.250		0.250		0.250		
18.1	$\frac{9}{2}^+$	0.125				0.063	0.125		
		0.125					0.125		
19.5	$\frac{5}{2}^-$	0.500				0.500			
		0.500				0.500			

assignments represent the best choices at each energy. In all cases, for other choices of J^π, the fit would not rise anywhere near the data. Also, in the final stages of the fitting process, each level was removed in the same order that it was added and other J^π values were again attempted, but the original assignments resulted in the best fits.

Hausladen *et al.*[19] made a probable assignment of $\frac{3}{2}^+$, $\frac{5}{2}^+$, $\frac{7}{2}^+$ to the level at $E_x = 15.2$ MeV. The present work indicates that two positive parity levels are in the region. The $\frac{5}{2}^+$ is needed for B_0 for scattering to the second excited level in ^{10}B, and through interference with the $\frac{7}{2}^+$ it is also needed at $E_n = 4.5$ MeV to cause the resonance in B_4 for scattering to the third excited level in ^{10}B. When either of these levels is removed, the B_4 coefficient for scattering to the third excited level in ^{10}B vanishes. Rihet[28] made a probable assignment of $\frac{1}{2}^+$, $\frac{3}{2}^+$, $\frac{5}{2}^+$ for a level in ^{11}C that would correspond to a 15.6 MeV level in ^{11}B. Brown[12] has predicted a $\frac{7}{2}^+$ level at 15.22 MeV and a $\frac{5}{2}^+$ at 15.42 MeV. Both Refs. 3 and 24 have predicted a $\frac{5}{2}^+$ at 15.8 MeV, and Ref. 24 has also predicted $\frac{5}{2}^+$ levels at 15.1 and 15.5 MeV.

The $\frac{9}{2}^-$ level at 15.8 MeV is a very strongly interfering level. Without it, no other J^π could bring the fit for the elastic B_1 or the B_0 coefficient for scattering to the first excited level in ^{10}B around 2 to 3 MeV close to the data. It is also partly responsible for the dip in all elastic coefficients at 3.8 MeV. Evidence of its interference with

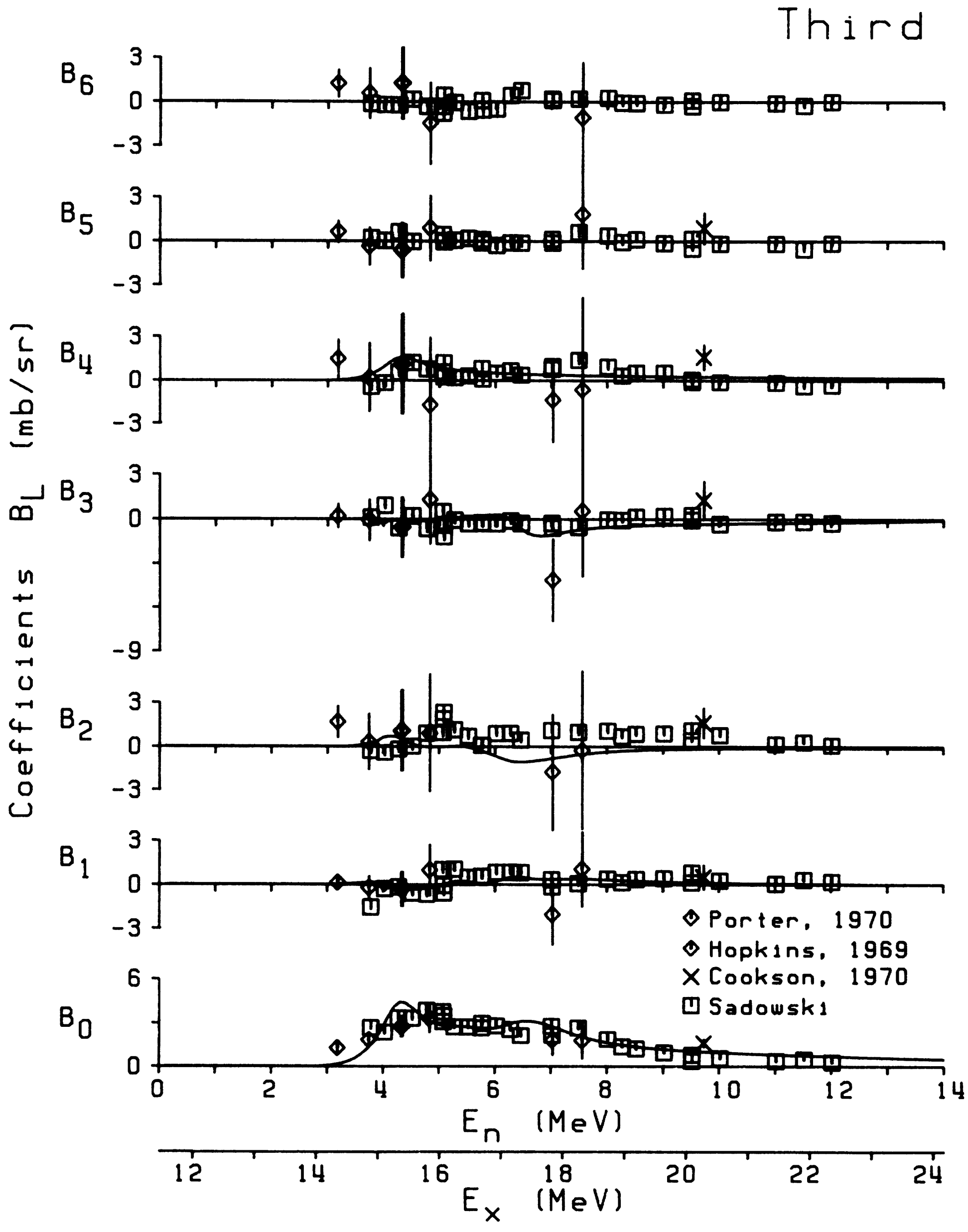

FIG. 10. Legendre polynomial coefficients for inelastic scattering to the third excited state of ^{10}B. See caption for Fig. 7.

the $\frac{5}{2}^+$ and $\frac{7}{2}^+$ levels of this region can be seen in B_1 for scattering to the first excited level in ^{10}B and both B_1 and B_3 for scattering to the third excited level in ^{10}B. Most theory calculations have no $\frac{9}{2}^-$ level in this region. Cavaignac *et al.*[15] analyzed ^{11}B$(p,p')^{11}$B scattering for $E_p = 30$ MeV by coupling hole states to ^{12}C core states in the framework of the unified model with coupling of the $K=\frac{1}{2}$ and $K=\frac{3}{2}$ bands. A $\frac{9}{2}^-$ level was calculated at 16.44 MeV in this analysis.

In the elastic coefficients, the $\frac{7}{2}^-$level at 16.5 MeV was partly responsible for the broad dip around $E_n = 6$ MeV, while it causes large peaks in the B_0 coefficients and B_2 coefficients for scattering to the first and fourth excited levels in ^{10}B. Contrary to the $\frac{9}{2}^-$ case, several theoretical predictions place $\frac{7}{2}^-$ strength in the area. Brown[12] predicted two levels, at 15.56 and 17.81 MeV. Clegg[13] also predicted two levels at 16.1 and 17.1 MeV. Norton and Goldhammer[5] predicted a single $\frac{7}{2}^-$ at 16.4 MeV. Cohen and Kurath[2] predicted at $\frac{7}{2}^-$ at 15.08 MeV with $\theta_{\lambda\,\mathrm{elas}} = 0.109$. $\theta_{\lambda\,\mathrm{elas}}$ from the present work was 0.276.

The final negative parity level, a $\frac{5}{2}^-$ at 16.9 MeV, affected coefficients for all the inelastic reactions studied. This level interfered constructively with the $\frac{7}{2}^-$ from above in all the inelastic cross sections. Without this level, the B_0 and B_2 coefficients for scattering to the first excited level of ^{10}B were smaller than the data. Brown,[12]

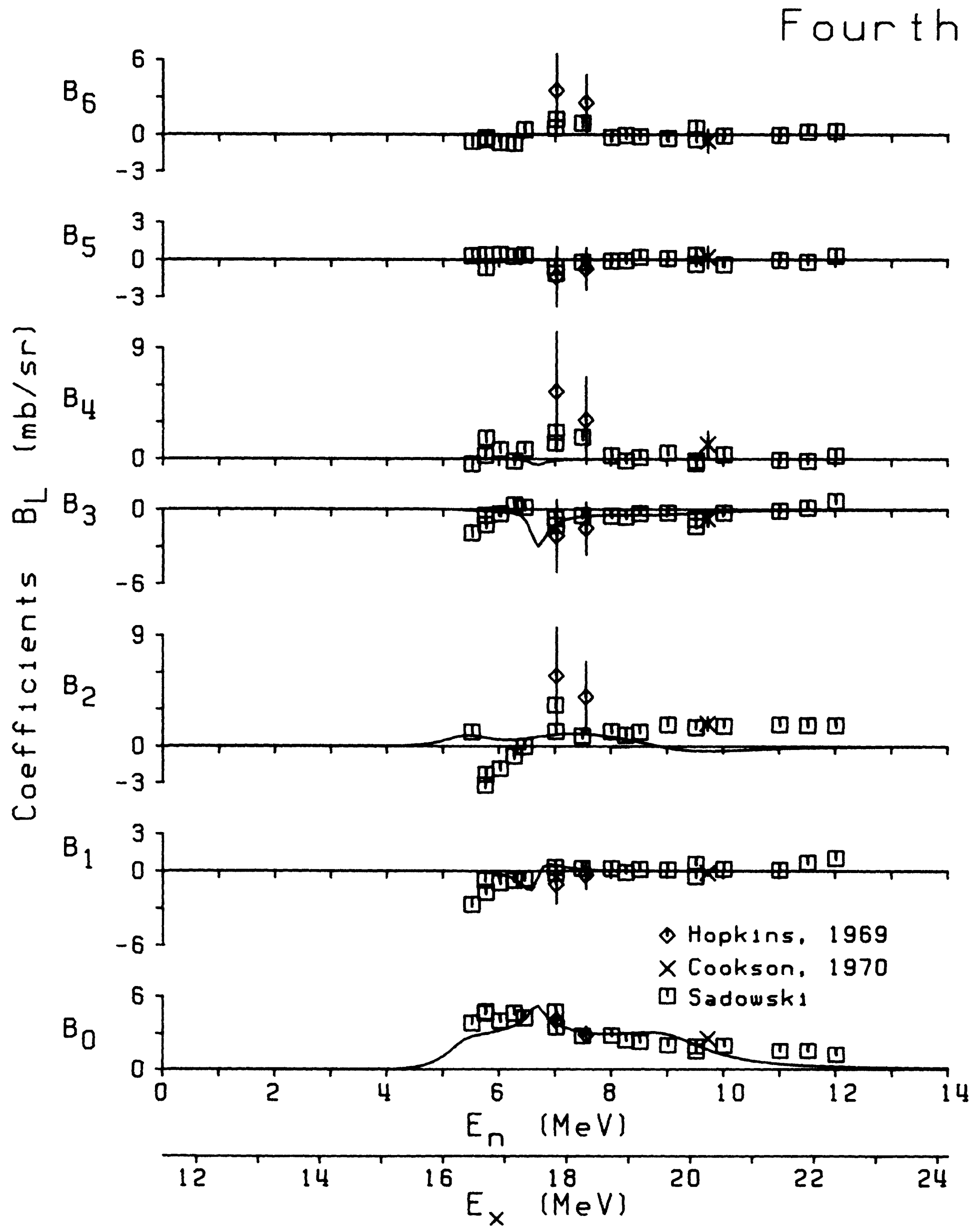

FIG. 11. Legendre polynomial coefficients for inelastic scattering to the fourth excited state of ^{10}B. See caption for Fig. 7.

Sorokin *et al.*,[24] and Boyarkina[1] all predicted a single $\frac{5}{2}^-$ level within 500 keV of 16.9 MeV.

D. $E_x > 17$ MeV ($E_n > 6.1$ MeV)

In this region of very broad levels, the cross sections for different reactions behaved somewhat differently. The one feature common to all the reactions was that again both even and odd coefficients were excited, so both positive and negative parity levels were interfering. The B_0–B_4 coefficients for elastic scattering showed a very broad resonance centered around $E_n \approx 7$ MeV. The cross section for scattering to the first and second excited levels of ^{10}B decreased with energy and showed very little structure. The remaining inelastic cross sections, while generally also decreasing, displayed structure in the higher coefficients.

The only combination of positive parity and negative parity levels that resulted in a fit anywhere close to the large peaks in the cross section for scattering to the fifth excited level of ^{10}B while maintaining the relatively smooth behavior of the elastic cross section was a $\frac{9}{2}^-$ at 17.8 MeV, a $\frac{7}{2}^-$ at 17.9 MeV, and a $\frac{9}{2}^+$ at 18.1 MeV. Any other J^π added a very sharp "kink" in all the elastic coefficients and very little amplitude in the inelastic coefficients. The $\frac{9}{2}^-$ also added to the B_0–B_4 coefficients for scattering to the first, third, and fourth excited levels of ^{10}B around $E_n \approx 7$ MeV. From a study of the

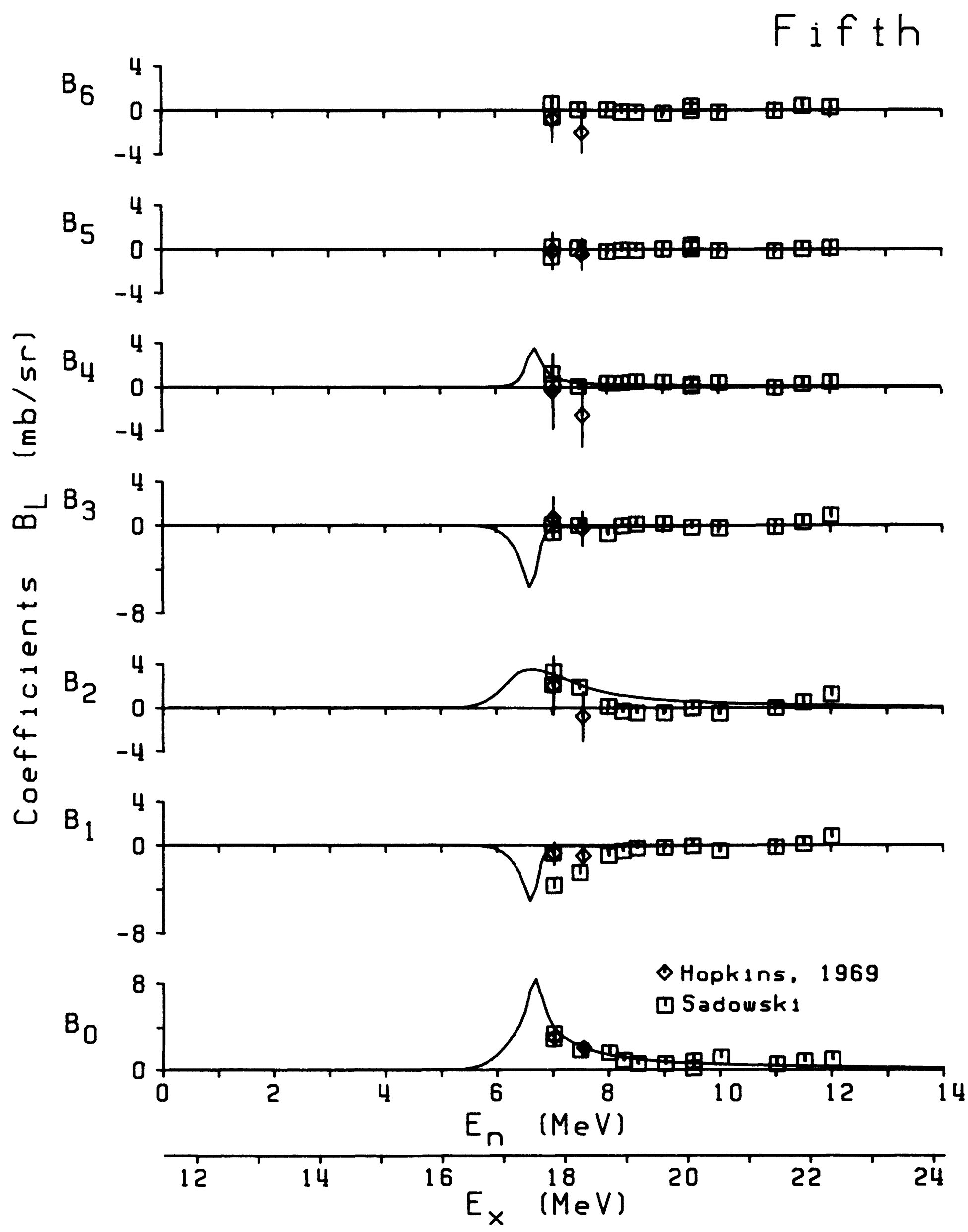

FIG. 12. Legendre polynomial coefficients for inelastic scattering to the fifth excited state of ^{10}B. See caption for Fig. 7.

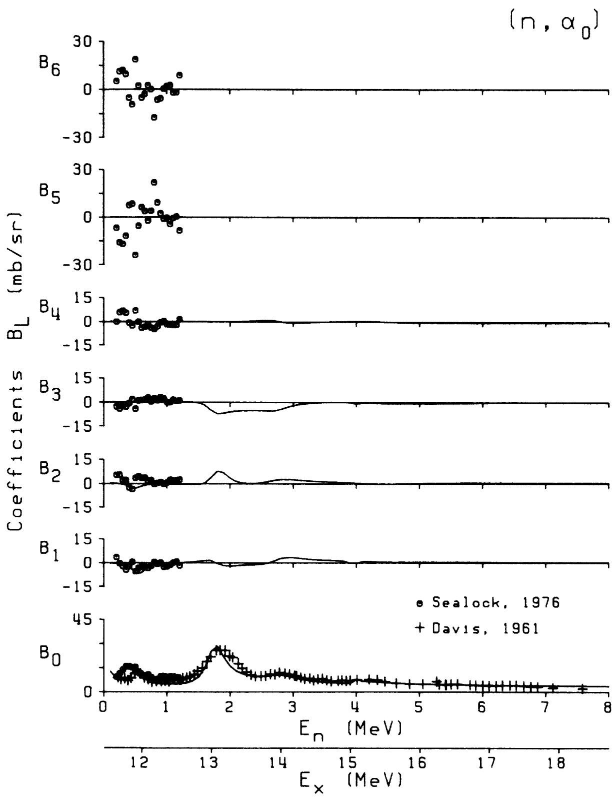

FIG. 13. Legendre polynomial coefficients for the reaction $^{10}B(n,\alpha_0)^7Li$. See caption for Fig. 7. For clarity, the errors on the data of Sealock, 1976, were omitted since those errors are so large as to cause overlapping of the graphs.

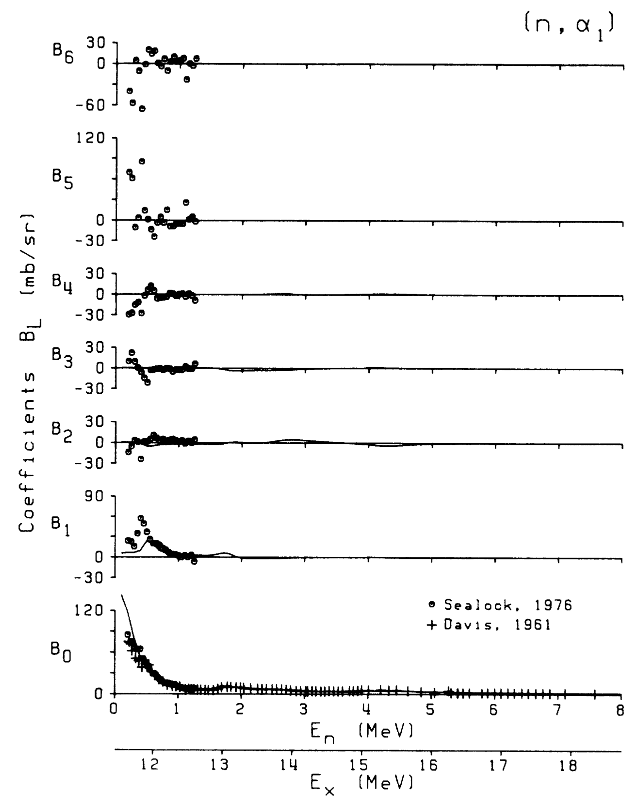

FIG. 14. Legendre polynomial coefficients for the reaction $^{10}B(n,\alpha_1)^7Li^*$. See caption for Fig. 7. For clarity, the errors on the data of Sealock, 1976, were omitted since those errors are so large as to cause overlapping of the graphs.

$^9Be(d,p_0)^{10}Be$ and $^9Be(d,p_1)^{10}Be^*$ reactions, Deinenko *et al.*[53] concluded that the spin of the two levels at $E_x = 17.3$ and 17.7 MeV must be $\geq \frac{9}{2}$. Cohen and Kurath[2] calculated the $\theta_{\lambda\,\text{elas}}$ for a $\frac{9}{2}^-$ level at 19.67 MeV to be 0.022, while the present work found $\theta_{\lambda\,\text{elas}}$ to be 0.180. Brown[12] predicted a $\frac{9}{2}^+$ level at 18.48 MeV, and van Hees and Glaudenmans[11] predicted a $\frac{9}{2}^+$ level to be at 16.9 MeV.

The $\frac{7}{2}^-$ level at 17.9 MeV mostly affected the cross section for scattering to the second (B_0 and B_2), third, and fifth excited levels of ^{10}B. For the third excited level, the $\frac{7}{2}^-$ interfered with just about every nearby level since it differed from them by only one or two units of angular momentum. The most notable effects were in B_1 and B_3 where this level interfered destructively to bring the fit near the data. The cross section for scattering to the fifth excited level of ^{10}B was most affected by the addition of this level. For all coefficients, B_0 to B_4, the calculated values became very large and the peaks became narrower, corresponding more closely to the data. Several theoretical calculations place a $\frac{7}{2}^-$ level in this area: Clegg[13] at 17.1 MeV, van Hees and Glaudenmans[11] at 17.9 MeV, and Brown[12] at 17.81 MeV.

The final assignment in this work was a $\frac{5}{2}^-$ level at 19.5 MeV. This level was added to raise the calculated cross section for scattering to the fourth excited level of ^{10}B around $E_n \approx 9.0$ MeV. Again, a single $\frac{5}{2}^-$ level was the most effective at accomplishing this purpose. Norton

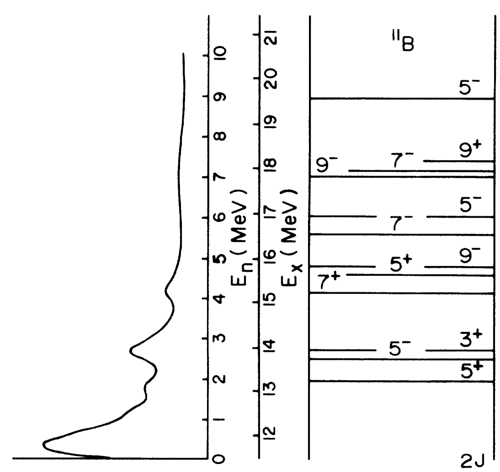

FIG. 15. The ^{11}B level diagram illustrating the new spin and parity assignments from the present study. The angle-integrated elastic cross section is also shown for reference.

and Goldhammer[5] (18.34 MeV), El-Batanoni *et al.*[14] (20.18 MeV), and Brown[12] (18.51 and 20.35 MeV) all predicted a $\frac{5}{2}^-$ level in this region.

Figure 15 is a level diagram of ^{11}B illustrating the assignments proposed by the present study.

V. CONCLUSIONS

New information for the level structure of ^{11}B has been deduced from R-matrix analyses of the present measurements of elastic and inelastic neutron scattering from ^{10}B, as well as from previous (n,α) data. The new results are summarized in Fig. 15 and in Tables I–V. The new levels that were studied were all broad, which was expected since ^{11}B can decay through a variety of particle channels for $E_x > 13$ MeV. Because of this, energies, widths, and assignments for only the most prominent levels were extracted in the present work. Comparison to model predictions have been made in a number of cases with reasonable agreement in several of them.

ACKNOWLEDGMENTS

The authors would like to express their appreciation to B. A. Brown for providing us with his unpublished ^{11}B shell model calculations. We are indebted to David Sturbois and Donald Carter of the accelerator staff for their many hours of hard work which were required for the completion of the experimental work. We also thank John O'Donnell for his help with computer-related aspects of this work. This work was supported by the U.S. Department of Energy.

---

*Present address: Westinghouse Savannah River Company, Aiken, SC 29808.
†Present address: Knolls Atomic Power Laboratory, General Electric Company, Schenectady, NY 12301.
‡Present address: Lawrence Livermore National Laboratory, Livermore, CA 94550.

[1]A. N. Boyarkina, Izv. Akad. Nauk SSSR, Ser. Fiz. **28**, 335 (1964).
[2]S. Cohen and D. Kurath, Nucl. Phys. **A101**, 1 (1967).
[3]I. V. Kurdyumov and Yu. F. Smirnov, Moscow Univ. Phys. Bull. **23**, 63 (1968).
[4]S. Cohen and D. Kurath, Nucl. Phys. **A141**, 145 (1970).
[5]J. L. Norton and P. Goldhammer, Nucl. Phys. **A165**, 33 (1971).
[6]B. M. Spicer and R. F. Fraser, Aust. J. Phys. **26**, 7 (1973).
[7]H. U. Jäger and M. Kirchbach, Nucl. Phys. **A291**, 52 (1977).
[8]W. D. Teeters and D. Kurath, Nucl. Phys. **A275**, 61 (1977).
[9]W. D. Teeters and D. Kurath, Nucl. Phys. **A283**, 1 (1977).
[10]N. G. Goncharova, B. S. Ishkhanov, and V. I. Mokeev, Yad. Fiz. **35**, 43 (1982) [Sov. J. Nucl. Phys. **35**, 26 (1982)].
[11]A. G. M. van Hees and P. W. M. Glaudemans, Z. Phys. A **315**, 223 (1984).
[12]B. A. Brown, private communication (1988).
[13]A. B. Clegg, Nucl. Phys. **38**, 353 (1962).
[14]F. El-Batanoni and A. A. Kresnin, Nucl. Phys. **89**, 577 (1966).
[15]J. F. Cavaignac, S. Jang, and D. H. Worledge, Nucl. Phys. **A243**, 349 (1975).
[16]F. Brut and S. Jang, Phys. Rev. C **14**, 1638 (1976).
[17]I. Ragnarsson, S. Åberg, H. B. Hakansson, and R. K. Sheline, Nucl. Phys. **A461**, 1 (1981).
[18]F. Ajzenberg-Selove, Nucl. Phys. **A433**, 1 (1985).
[19]S. L. Hausladen, C. E. Nelson, and R. O. Lane, Nucl. Phys. **A217**, 563 (1973).
[20]B. Zwiegliński, W. Benenson, G. M. Crawley, S. Gales, and D. Weber, Nucl. Phys. **A389**, 301 (1982).
[21]K. Locker and P. Stoll, Nucl. Phys. **90**, 164 (1953).
[22]P. Kossanyi-Demay and G. J. Vanpraet, Nucl. Phys. **A81**, 529 (1966).
[23]D. R. Goosman, E. G. Adelberger, and K. A. Snover, Phys. Rev. C **1**, 123 (1970).
[24]Yu. I. Sorokin, A. Kh. Shardanov, V. G. Shevchenko, and B. A. Yur'ev, Yad. Fiz. **11**, 8 (1970) [Sov. J. Nucl. Phys. **11**, 4 (1970)].
[25]K. Battelson and D. K. McDaniels, Phys. Rev. C **14**, 1601 (1971).
[26]B. A. Watson, C. C. Chang, and M. Hasinoff, Nucl. Phys. **A173**, 634 (1971).
[27]A. S. Alimov, V. I. Mokeev, E. S. Omarov, and I. M. Piskarev, Yad. Fiz. **40**, 301 (1984) [Sov. J. Nucl. Phys. **40**, 190 (1984)].
[28]Y. Rihet, Ph.D. dissertation, Louis Pasteur University of Strasbourg, France (1984).
[29]R. Aryaeinejad, W. R. Falk, N. E. Davison, J. N. Knudson, and J. R. Campbell, Nucl. Phys. **A436**, 1 (1985).
[30]G. F. Auchampaugh, S. Plattard, and N. W. Hill, Nucl. Sci. Eng. **69**, 30 (1979).
[31]J. C. Hopkins and D. M. Drake, Nucl. Sci. Eng. **36**, 275 (1969).
[32]J. A. Cookson and J. G. Locke, Nucl. Phys. **A146**, 417 (1970).
[33]D. Porter, R. E. Coles, and K. Wyld, AWRE Report No. 045/70 Aldermaston, 1970 (unpublished).
[34]H. D. Knox, Ohio University Internal Report, 1985 (unpublished).
[35]S. G. Glendinning, S. El-Kadi, C. E. Nelson, R. S. Pedroni, F. O. Purser, R. L. Walter, A. G. Beyerle, C. R. Gould, L. W. Seagondollar, and P. Thambidurai, Nucl. Sci. Eng. **80**, 256 (1982).
[36]M. Drosg, P. W. Lisowski, D. M. Drake, R. A. Hardekopf, and S. M. Muellner, LANL Report No. LA-10665-MS, 1986 (unpublished).
[37]D. O. Nellis, W. E. Tucker, and I. L. Morgan, Phys. Rev. C **1**, 847 (1970).
[38]R. B. Day and M. Walt, Phys. Rev. **117**, 1330 (1960).
[39]E. T. Sadowski, Ph.D. dissertation, Ohio University (1988).
[40]D. A. Resler and E. T. Sadowski, Nucl. Instrum. Methods **A269**, 607 (1988).
[41]B. Antolkovic, J. Hudomalj, B. Janko, G. Paic, and M. Turk, Nucl. Phys. **A139**, 10 (1969).
[42]H. G. Bingham, K. W. Kemper, and N. R. Fletcher, Nucl. Phys. **A175**, 374 (1971).
[43]K. Murphy, in *Nuclear Data for Basic and Applied Science*, Proceedings of the International Conference, Sante Fe, New Mexico, 1985, edited by P. G. Young, R. E. Brown, G. F. Auchampaugh, P. W. Lisowski, and L. Stewart (Gordon and Breach, New York, 1986), Vol. 1, p. 219.
[44]P. E. Koehler, H. D. Knox, D. A. Resler, R. O. Lane, and G.

F. Auchampaugh, Nucl. Phys. **A453**, 429 (1986).
[45]D. A. Resler, H. D. Knox, P. E. Koehler, R. O.Lane, and G. F. Auchampaugh, Phys. Rev. C **39**, 766 (1989).
[46]T. Teichmann and E. P. Wigner, Phys. Rev. **87**, 123 (1952).
[47]A. M. Lane, private communication (1978).
[48]C. B. Dover, C. Mahaux, and H. A. Weidenmüller, Nucl. Phys. **A139**, 593 (1969).
[49]A. M. Lane and R. G. Thomas, Rev. Mod. Phys. **30**, 257 (1958).
[50]R. O. Lane, S. L. Hausladen, J. E. Monahan, A. J. Elwyn, F. P. Mooring, and A. Langsdorf, Jr., Phys. Rev. C **4**, 380 (1971).
[51]H. Furutani, H. Kanada, T. Kanecko, S. Nagata, H. Nishioka, S. Okabe, S. Saito, T. Sakuda, and M. Seya, Prog. Theor. Phys. Suppl. **68**, 193 (1980).
[52]E. I. Dubovoi, Yad. Fiz. **12**, 965 (1970) [Sov. J. Nucl. Phys. **12**, 526 (1971)].
[53]A. S. Deinenko, I. I. Zalyubovskii, I. Ya. Malakhov, V. D. Sarana, V. E. Storizhko, and N. A. Salyakhov, Bull. Acad. Sci. USSR Phys. Ser. **44**, 163 (1980).